



A novel ceramifiable epoxy composite with enhanced fire resistance and flame retardance

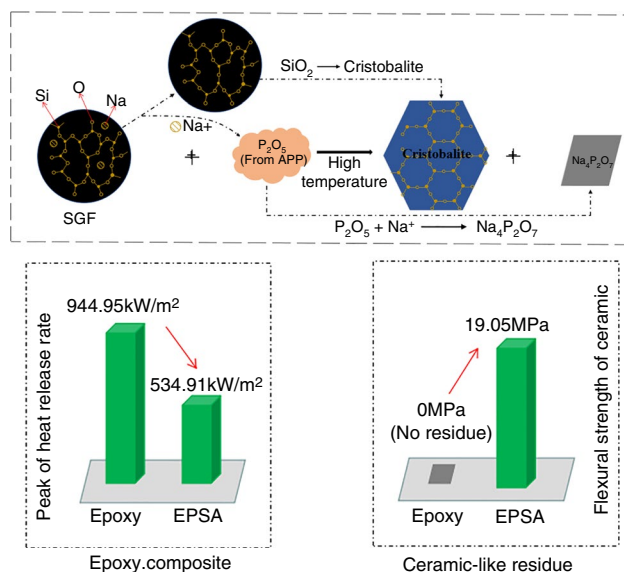
Dong Zhao^{1,2} · Wei Liu^{1,2} · Yucai Shen^{1,2} · Tingwei Wang^{1,3}

Received: 8 January 2020 / Accepted: 19 August 2020 / Published online: 15 September 2020
© Akadémiai Kiadó, Budapest, Hungary 2020

Abstract

A novel epoxy composite with flame retardance and fire resistance was prepared by adding silicate glass frit (SGF) and ammonium polyphosphate (APP) into the epoxy resin. In the combustion test, epoxy composites displayed obvious flame retardance feature, showing much lower heat release rate, total heat release and total smoke production than epoxy resin. The composite residue formed at 900 °C had a flexural strength of 19.05 MPa. In addition, possible mechanisms for the phase separation and crystallization reactions at high temperatures were also investigated in detail through thermogravimetric analyzer, X-ray diffraction, X-ray photoelectron spectrometer, and scanning electron microscopy. It was suggested that phosphorus element tends to migrate to the surface of the composite residue during firing process, and sodium element from SGF is selectively combined with the phosphorus element to obtain crystalline phases. With this unique phase separation and crystallization reactions, the fire resistance of the epoxy composite was significantly improved.

Graphical abstract



Keywords Epoxy · Composites · Ceramifiable · Flame retardance · Fire resistance

Introduction

Epoxy resin is one of the most versatile thermosetting polymeric materials, which has a wide application in various fields owing to its excellent adhesive properties, satisfactory

Dong Zhao and Wei Liu have contributed equally to this work.

Extended author information available on the last page of the article

chemical resistance and good thermal and mechanical stability [1–5]. However, with a limiting oxygen index (LOI) of only 19.5%, epoxy resin is highly flammable, and there is almost no residue left after sufficient combustion, which severely restricts its further application for use as reinforcing material in structural engineering of building [6]. Consequently, it is imperative to improve the flame retardance and fire resistance of epoxy resin.

Although a great deal of work [7–11] has been devoted to improving the flame retardancy of epoxy composites through physically adding various flame retardants, it still cannot meet the use requirements in the long-lasting fire or high temperature (over 900 °C) conditions. In order to overcome this problem, strategies to make polymer composite ceramifiable in the fire are reported [12–17], and those ceramifiable composites have similar properties of matrix materials at room temperature, but they could be converted to ceramic-like residues when they are fired at high temperatures.

Many studies [18–22] have been implemented to achieve a high fire resistance in a polymer composite, and the main aim is to improve shape stability, self-supporting performance or strength of fired composite residue. Glass frit with a low softening point as flux agent was often added to the ceramifiable polymer composite system. With the increase in temperature, glass frit will melt into liquid phase and then adhere to other components together to form a compact ceramic residue. This is a relatively effective method, but this kind of ceramifiable composite will have serious deformations due to the strong liquidity of the glass frit at high temperatures [18–20]. Glass fibers or carbon fibers were added to construct a skeleton as the supporting structure of residues [21, 22]. Another approach [23–28] is to increase the crystal content of the residue, and this strategy has been applied in the ceramifiable silicone rubber composites and EVA composites. For example, Shen et al. [23] improved the ceramifiable properties of silicone rubber composite through incorporation of ammonium polyphosphate, aluminum hydroxide, and mica, resulting in crystallization reaction among these additives. Gong et al. [25] prepared ceramifiable EVA composites by adding whitened and capsulized red phosphorus (WCRP) and silicate glass frit. It showed that the addition of WCRP promoted the generation of cristobalite crystal, which led to an improvement in the self-supporting property of the composite at high temperatures. The key to obtain ceramifiable polymer composites seems to need specific additives that could react into certain reinforcing phase at firing temperature, but this is not easy to achieve experimentally for different polymer matrix. To the best of our knowledge, ceramifiable polymer composite is rarely reported for thermosetting system such as epoxy.

On the one hand, ammonium polyphosphate (APP) is an excellent non-halogen flame retardant and widely used in flame-retarding polymer materials [29–31]. Moreover,

ceramifiable property of polymer composite could also be improved due to the reaction between APP and other filler [17, 23, 24]. In our previous work [25], it was found that the interaction of phosphorous with some silicate compounds at high temperature is vital to improve fire resistance of the polymer composites. Thus, on the other hand, APP was used as a resource of phosphorus to induce the chemical reaction at high temperatures. In this study, a novel epoxy composite with high fire resistance was prepared by adding APP and silicate glass frit (SGF). The flame retardance of epoxy composite was tested by an oxygen index instrument and a cone calorimeter device. The fire resistance of the composite was investigated with the aid of shape stability test and flexural strength test. Furthermore, possible mechanisms for the phase separation and crystallization reactions at high temperatures were also investigated through TG, XRD, XPS, EDX, etc.

Experimental

Materials

The epoxy resin chosen here was liquid diglycidyl ether of bisphenol A (E51) obtained from Wuxi Bluestar Co., Ltd., and the curing agent methyl tetrahydrophthalic anhydride (MTHPA) was supplied by Zhejiang Alpha Chemical Technology Co., Ltd., and curing accelerator 2-ethyl-4-methylimidazole was purchased from Qingdao Haida chemical Co., Ltd. Silicate glass frit (SGF) was supplied by Kunshan Huaqiao Co., Ltd., which is composed of SiO₂: 66.32 mass % Na₂O: 19.76 mass % TiO₂: 6.12 mass % F: 3.71 mass % others: 3.09 mass %. Ammonium polyphosphate (APP) was purchased from JLS Flame Retardants Chemical Co., Ltd.

Sample preparation and pyrolysis

Epoxy composites were prepared as shown in Fig. 1. The preparation includes the following steps. Firstly, the mixture of epoxy resin and MTHPA (epoxy resin: MTHPA = 5:4, by mass ratio) was heated in oil bath at 85 °C under stirring. When the mixture was evenly mixed, 2-ethyl-4-methylimidazole was added to the above mixture with stirring. APP and SGF were then added with stirring for 20 min. Finally, the composite was cured in an oven at 145 °C for 4 h. The same method was used to prepare samples without APP as an experimental comparison. The formulations of samples are shown in Table 1. All samples were fired at 600, 700, 800, 900, and 1000 °C for 30 min in a muffle furnace, respectively.

Fig. 1 Schematic showing the preparation of epoxy/SGF/APP (EPSA) composite

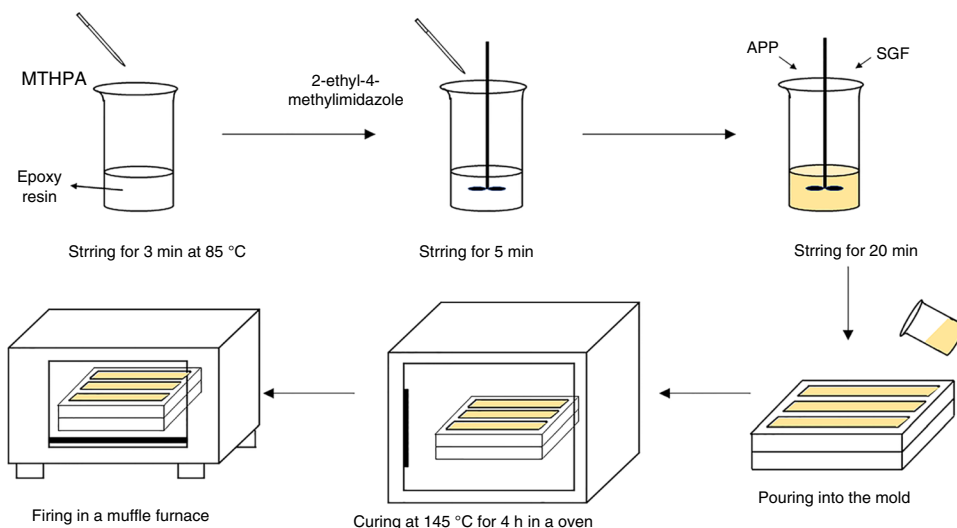


Table 1 Formulations of samples

Sample	Epoxy/g	MTHPA/g	2-ethyl-4-methylimidazole/g	SGF/g	APP/g
EP	8.55	6.84	0.05	–	–
EPS	8.55	6.84	0.05	24.61	–
EPSA	8.55	6.84	0.05	20.83	3.78

Characterizations

Impact strength was carried out on an Izod impact test machine (HT-503, Dongguan Hengtong, China) according to ASTM D4812–2006.

Limited oxygen index (LOI) values were tested on a HC-2 oxygen index instrument (Jiangning, China) with sheet dimensions of $100 \times 10 \times 4 \text{ mm}^3$ according to GB/T2406 standard; the vertical burning test (UL-94) was conducted using the vertical burning test instrument (CZF-2) (Nanjing Jion-glei Experimental Equipment Co., Ltd, Nanjing, Jiangsu, China) according to ASTM D 3801 standard.

Fire behavior of the samples was measured on $100 \times 100 \times 4 \text{ mm}^3$ sheets according to ISO 5660 by a standard cone calorimeter (Fire Testing Technology Ltd, Sussex, Britain). Samples were burned horizontally at a heat flux of 50 kW m^{-2} .

Linear shrinkage was calculated by measuring the length of the samples before and after firing at high temperatures. The linear shrinkage was calculated using Eq. (1):

$$L = (L_d - L_o) / L_d \times 100\% \quad (1)$$

where L is linear shrinkage (%), L_d is the dimensional length of sample after firing and L_o is the original length of the sample.

Universal testing machine (CMT-6203; MTS System Corporation, China) was used to test the flexural strength of residues by three-point bend mode, according to the GB/T9596-2006 standard.

Microstructure and elemental dispersion of samples were characterized by a scanning electron microscope (SEM; Japan Electronics Co. Ltd., China) equipped with an energy-dispersive X-ray (EDX; Thermal Scientific, USA) spectrometer.

XRD data were obtained from 5° to 65° at a scan rate of $10^\circ \text{ min}^{-1}$ to study the phase composition of the residues fired at different temperatures by an X-ray diffractometer (XRD; Rigaku Corporation, Japan).

Thermal gravimetric (TG; Netzsch instruments Co., Germany) analysis was conducted on a thermal analyzer from room temperature to 800° C (nitrogen atmosphere, heating rate of $10^\circ \text{ C min}^{-1}$).

X-ray photoelectron spectroscopy (XPS; TFS Escalab 250Xi, USA) to identify the electronic state of the residues.

Results and discussion

Morphology analysis

The morphology of residues of EPS and EPSA fired at different temperatures is shown in Fig. 2. After firing at 1000° C , EPS had a significant deformation due to the high flow capacity of the melted SGF. By contrast, the original shape of EPSA fired at 1000° C can still be maintained, indicating that the fire resistance of the composite is significantly improved due to the addition of APP. In addition, the carbonization of polymer matrix is considered a significant factor for the blackness of the residues [32]. It is worth noting that the surface of EPSA residues became flat and

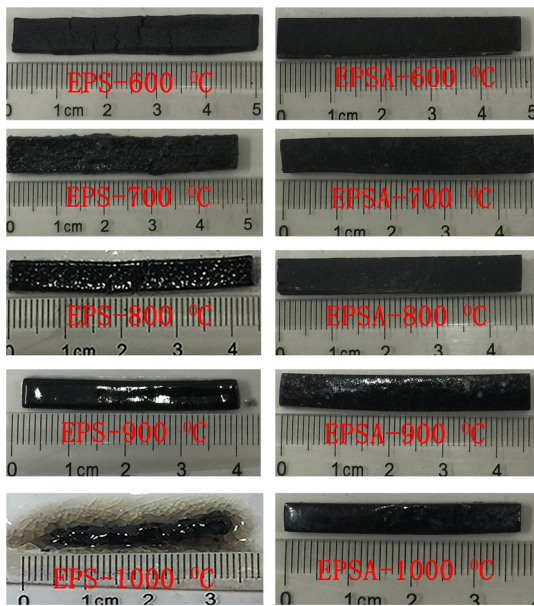


Fig. 2 Surface morphology of EPS (left) and EPSA (right) fired at different temperatures

Table 2 Impact strength of EP and epoxy composites

Sample	Impact strength/ kJ m^{-2}
EP	25.70
EPS	3.93
EPSA	3.72

smooth with the increase in temperature, because SGF was melted into liquid phase at the surface of the sample.

Mechanical properties of epoxy composites and residues

Mechanical properties of epoxy composites

The impact strength of samples EP, EPS, and EPSA is shown in Table 2. For the EP, the impact strength is 25.70 kJ m^{-2} . When SGF and APP were added to epoxy resin, the impact strength decreased, and this may result from the poor compatibility between the epoxy resin and inorganic fillers [33, 34]. The impact strength of EPS and EPSA was similar; both are larger than 4 kJ m^{-2} .

Mechanical properties of ceramic residues

Composites residues of sample EPS fired at 800, 900, and 1000 °C adhered to the surface of refractory bricks. Hence, the flexural strength of EPS residues was not tested. The

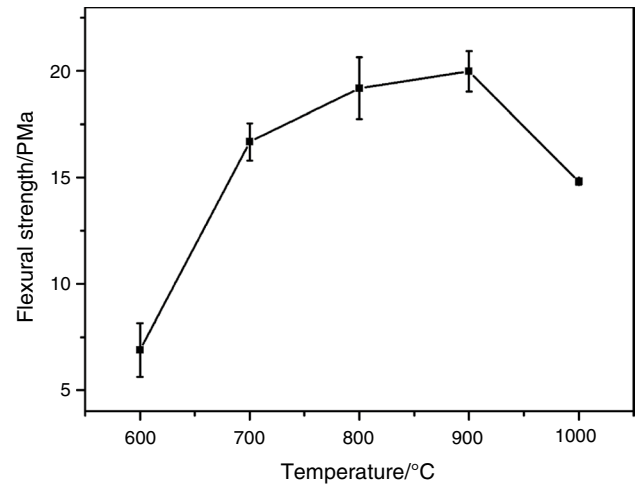


Fig. 3 Flexural strength of EPSA fired at different temperatures

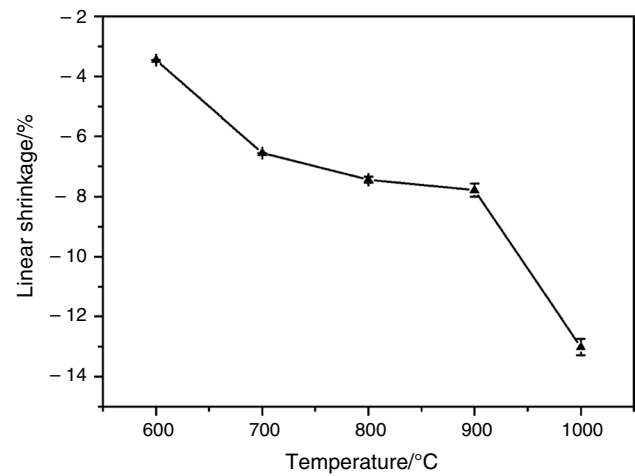


Fig. 4 Line shrinkage of EPSA fired at different temperatures

flexural strength of the EPSA fired at various temperatures is shown in Fig. 3. When the temperature increased from 600 to 900 °C, an increase in the flexural strength of EPSA residues is observed, which may result from more liquid phase produced by melting SGF, and that is beneficial to generate denser residue structures. The flexural strength of the EPSA residue was significantly improved at the temperature from 600 to 700 °C. However, there is an obvious decrease in the flexural strength of the ceramic residues at the temperature from 900 to 1000 °C, which may result from the reduction in the liquid phase in the residue.

Linear shrinkage analysis

Figure 4 shows the linear shrinkage of EPSA fired at various temperatures. The linear shrinkage of EPSA increased with increasing temperature. The melting temperature of SGF is

around 660 °C, when the firing temperature is higher than that, SGF will melt into liquid phase and could fill the pores formed by the decomposition of EP and APP, [27] which leads a significant increase in the linear shrinkage of the composite. There is a more significant increase in the linear shrinkage of samples fired from 900 to 1000 °C, possibly due to crystallization reaction [24, 35]. The crystallization reaction led to the reduction in liquid phase in the residues. Liquid phase as binding phase of residues can improve the density of the ceramic-like residue. Thus, decreased liquid phase led to a decrease in the flexural strength of the ceramic residue.

Combustion performance of epoxy composites

The LOI and UL-94 results of samples EP, EPS, and EPSA are shown in Table 3. The epoxy resin was easily

Table 3 LOI and UL-94 results of EP and epoxy composites

Sample	LOI/ %	UL-94
EP	19.5	Dripping (NC)
EPS	28.5	No dripping (NC)
EPSA	24.5	No dripping (NC)

NC, Not classified without self-extinguish

flammable and its LOI value was 19.5%. When SGF was incorporated into EP, the LOI of sample EPS increased to 28.5%, indicating that SGF had an influence on the flammability of epoxy resin. When APP was added to EPS, the LOI of sample EPSA slightly decreased to 24.5%. It can be seen from Table 3 that EP has serious melt dripping. Samples EPS and EPSA, however, are out of burning drip. Unfortunately, EPS and EPSA exhibit no rating without self-extinguish in the UL-94 vertical burning test. Obviously, SGF and APP promoted the flame retardance of the epoxy resin.

Cone calorimeter test was also applied to assess the combustible behaviors of samples. The cone calorimeter results are shown in Fig. 5 and Table 4. Compared to epoxy resin, the ignition time for samples EPS and EPSA was extended, illustrating that the fire safety of samples EPS and EPSA is higher than that of epoxy resin. Cone calorimeter result confirmed that epoxy resin was flammable. After ignition, a very sharp peak of heat release rate (PHRR) of 944.95 kW m⁻² and its total heat release (THR) and total smoke production (TSP) were 112.05 MJ m⁻² and 47.45 m², respectively. For sample EPS, the PHRR and THR were 359.73 kW m⁻² and 54.28 MJ m⁻², respectively. For sample EPSA, the PHRR and THR were

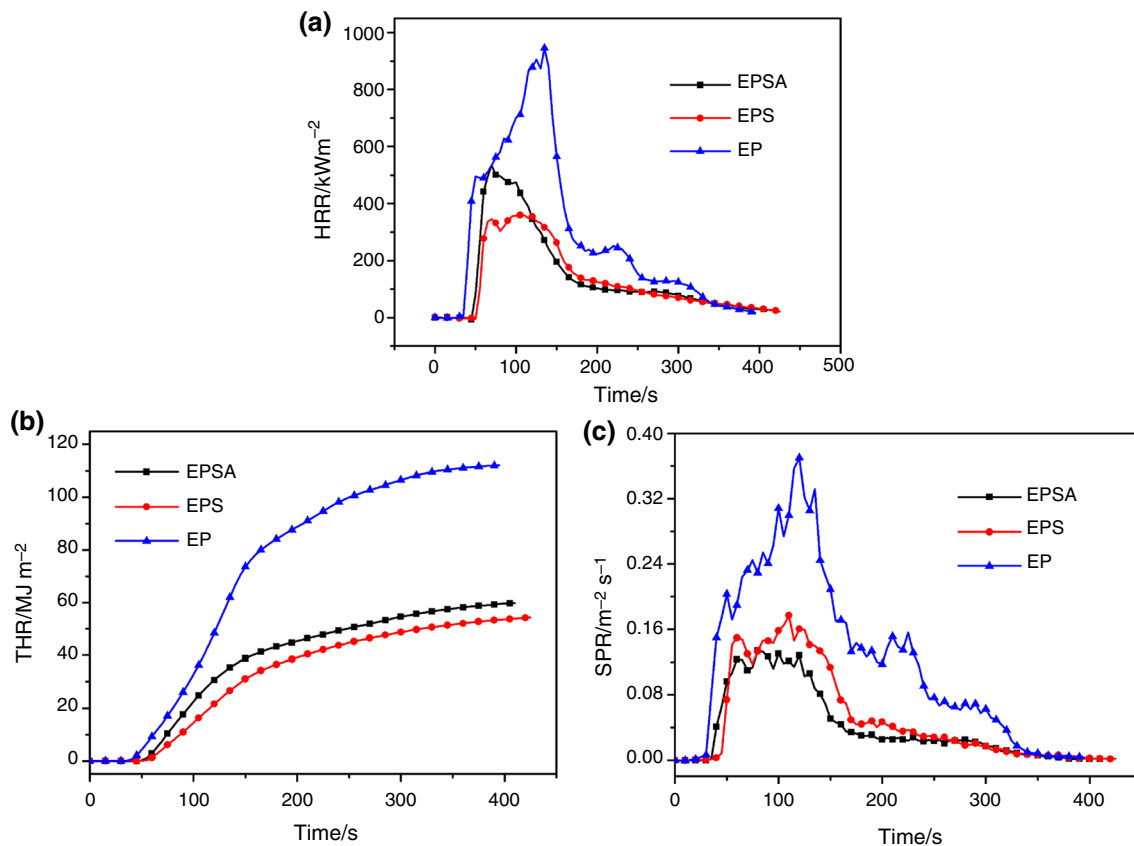


Fig. 5 Cone calorimetric curves of EP, EPS, and EPSA, HRR (a), THR (b), and SPR (c)

Table 4 Cone calorimetric data of EP and ceramifiable epoxy composites

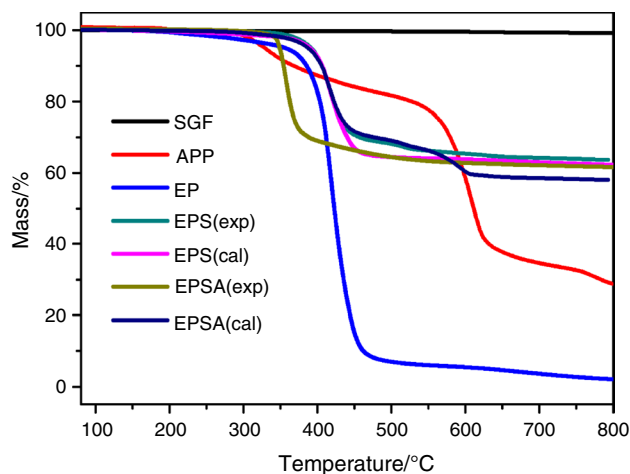
Sample	EP	EPS	EPSA
TTI/s	34	48	46
PHRR/kW m ⁻²	944.95	359.73	534.91
THR/MJ m ⁻²	112.05	54.28	59.83
TSR/m ² m ⁻²	5367.99	2378.19	1874.55
TSP/m ²	47.45	21.01	16.57

534.91 kW m⁻² and 59.83 MJ m⁻², respectively. Obviously, both the PHRR and THR values of samples EPS and EPSA decreased significantly in comparison with the corresponding values of epoxy resin. The TSP values of samples EPS and EPSA were only 21.01 m² and 16.57 m², respectively, which is much lower than that of epoxy resin. Obviously, SGF and APP exhibited a high efficiency in reducing the smoke release.

The char layer and ceramic-like layer could contribute to the flame retardation of epoxy composite, which would be an important reason for better flame retardance of samples EPS and EPSA than that of epoxy resin [36, 37]. Unfortunately, although the flame retardance of epoxy composite only adding SGF is much better than that containing SGF and APP from the data of LOI and CONE, the fire resistance of EPS cannot meet the usage requirement in some special fields. This may be due to the release of NH₃ and H₂O in the pyrolysis process of sample EPSA, which damaged the retardant layer to some extent [17].

Thermogravimetric analysis

The TG curves of pure SGF, pure APP, EP, EPS, and EPSA are shown in Fig. 6, and the corresponding data are summarized in Table 5. During the thermal degradation process of the pure SGF, it can be observed that the mass loss was less than 1%. Unlike the pure SGF, the thermal degradation of APP consisted of two mass loss steps. The first step of thermal degradation temperature of pure APP started at 295 °C and ended at 469 °C, owing to the release of NH₃ and H₂O. The second step from 544 to 683 °C was attributed to the decomposition and volatilization of P-O compounds [24, 38, 39]. It can be seen that the thermal degradation process of EP started at 278 °C and ended at 444 °C, and the mass of the residue was close to zero. Comparing the thermal decomposition temperature characteristics of EP and pure APP, it can be concluded that the EP was decomposed at a certain temperature accompanied by partial APP decomposition.

**Fig. 6** Thermal behaviors of SGF, APP, EP, EPS, and EPSA under nitrogen atmosphere**Table 5** Thermal characteristics of SGF, APP, EP, EPS, and EPSA

Sample	Temperature/°C		Mass remaining at 750 °C/ %
	First step	Second step	
SGF	–	–	99.25
APP	295–469	544–683	28.79
EP	278–444	–	2.71
EPS (exp)	328–475	–	63.88
EPS (cal)	326–467	–	61.08
EPSA (exp)	323–409	–	61.86
EPSA (cal)	294–475	542–618	55.45

Phosphoric acid was first formed after the first step decomposition of APP according to Jiang's research,³⁶ and the char decomposed by EP was coated with phosphoric acid. Moreover, the initial decomposition temperature of EPS was 328 °C much higher than 278 °C of EP. It indicates that the initial thermal decomposition temperature of EPS was delayed, which is attributed to the presence of silica in the SGF [40–42]. Further, comparisons between the experimental and calculated mass remaining of EPS and EPSA are shown in Table 2. The experimental mass remaining of EPS was higher than the calculated mass, suggesting that the addition of SGF can promote the char yield of EP. Similarly, the experimental mass remaining of EPSA was also higher than the calculated mass, indicating that the APP in composite could be able to further increase the mass of the residue.

Theoretically, EPSA sample would undergo two steps of thermal decomposition process due to the addition of APP, and the second step was caused by the decomposition

and volatilization of P-O compounds. However, thermal degradation of EPSA sample only consisted of one step in the real experiment, which indicates that the thermal stability of the composite was improved. As the temperature was further increased, the char was further retained in the residue due to the effect of adhesion of molten SGF, leading to the black residues as shown in Fig. 2. Moreover, phosphoric acid and the molten SGF on the surface of the composite lead to the production of dense ceramic-like barrier char and prevent combustible volatiles from escaping and burning in the fire zone.

SEM analysis of ceramic residues

Figure 7 shows the surface morphology of EPSA fired at high temperatures. The surface of EPSA fired at 600 °C showed porous structure, which is due to the release of NH₃, H₂O and CO₂ from the thermal degradation of APP and EP [23, 25]. However, the porous structures for EPSA fired at 800 °C obviously decreased, because the pores were filled with sufficient molten SGF liquid phase, leading to the smooth surface of the EPSA residue. Notably, the flexural strength of EPSA residues increased with the more compact structure of the residue. Compared with the surface morphology of EPSA fired at 800 °C, no significant liquid phase is observed on the surface of residue fired at 1000 °C. The residue exhibited a rough surface, which is not conducive to improve its mechanical properties, resulting in a decrease in flexural strength.

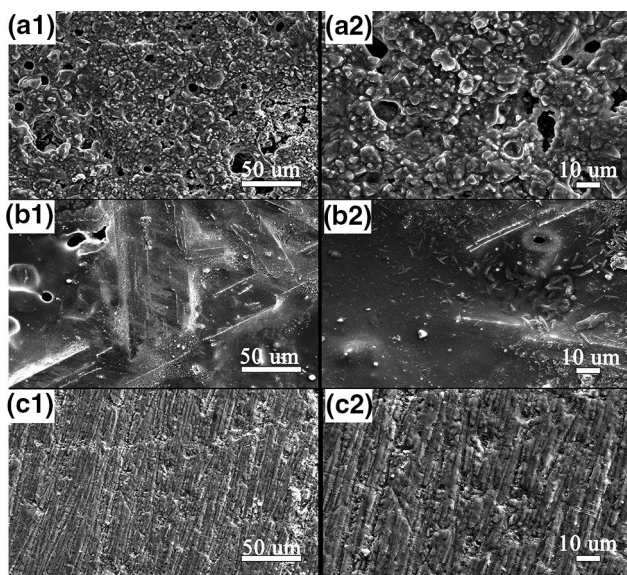
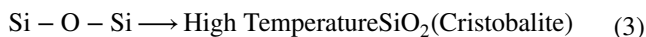
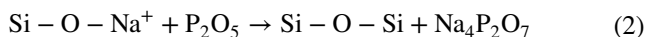


Fig. 7 Surface morphology of sample EPSA fired at 600, 800, and 1000 °C

XPS and XRD analysis for the residues at various temperatures

In order to investigate the interaction of the additives during firing process, the residue powder of EPSA fired at 800 °C, SGF powder and APP powder were tested by XPS. It is well known that silicon exists in the form of bridging silicon and non-bridging silicon. The Si2p XPS spectra of SGF powder and the ceramic residue powder of EPSA fired at 800 °C are shown in Fig. 8a, b. In Fig. 8a, the Si2p peaks at 102.3 and 102.8 eV corresponded to Si–O and Si–O–Na in SGF, which was a kind of silicon-terminal oxygen bond. However, for the residue powder of EPSA fired at 800 °C, there was a new Si2p peak appeared at 103.5 eV corresponding to the SiO₂, as shown in Fig. 8b. Si–O in SiO₂ was a kind of silicon-bridge oxygen bond. Hence, the chemical state of the silicon changed at high temperatures after adding APP [43, 44].

To confirm the effect of APP on the changing of chemical state of silicon, the XPS test was performed for APP. In Fig. 8c, P2p peaks at 134.2 and 135.7 eV corresponded to PO₄ and P₂O₅, while for the residue powder of EPSA fired at 800 °C, the binding energy of P2p (135.7 eV) disappeared. But a new P2p peak appeared at 133.2 eV attributing to the P₂O₇⁴⁻ [45]. It illustrated that the APP participated in the ceramization process. According to our previous research [24, 26], the sodium binding with non-bridge oxygen ions (such as ≡Si–O–) would be captured by phosphorus at high temperatures (Eq. 2). This promoted silicon-terminal oxygen bond changed into silicon-bridge oxygen bond (Eq. 3).



XRD was adopted to study the phase composition of SGF (Fig. 9) and EPSA (Fig. 10) fired at different temperatures. Figure 9 shows that there was only an amorphous “hump” can be observed, indicating that the phase composition of SGF fired at various temperatures was basically the same and no crystalline phase was shown [18, 24, 47]. For EPSA as shown in Fig. 10, some diffraction peaks appeared at positions of 20.07°, 26.45°, and 33.07°, fitting to the Na₄P₂O₇ phase [24]. It is worth noting that some new diffraction peaks appeared at 21.81, 28.28, 31.43, and 36.13° with increasing temperature, which confirmed the formation of cristobalite phase [48]. Further, the characteristic diffraction peaks at 21.81°, 28.28°, 31.43°, and 36.13° corresponded to (101), (111), (102), and (200) lattice planes of cristobalite crystal, respectively [49]. Therefore, the addition of APP led to a crystallization reaction.

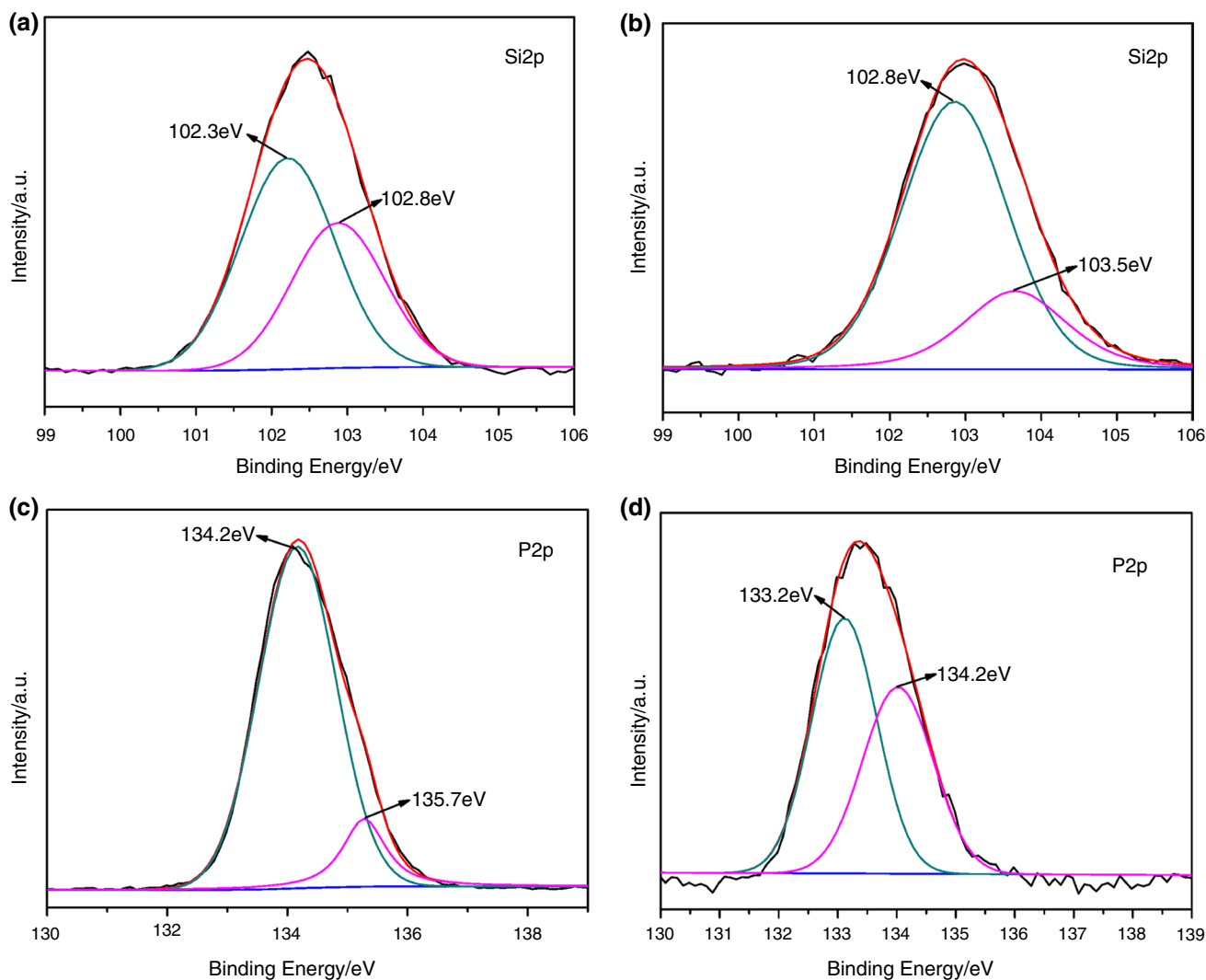


Fig. 8 XPS spectra of SGF (a), APP(c) and the residue of EPSA (b, d) fired at 800 °C

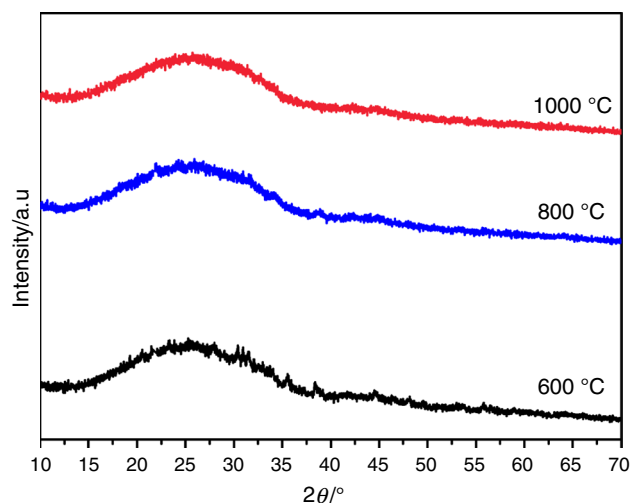


Fig. 9 XRD patterns of SGF fired at different temperatures

EDX analysis

Surface element composition of EPSA fired at 600, 800, and 1000 °C was analyzed by EDX, and the elemental mapping results are presented in Fig. 11. It can be observed that the content of silicon decreased gradually with the increasing temperature, whereas the content of phosphorus and sodium increased gradually. This indicated that phosphorus element migrated to the surface of the residue with increasing temperature. The migration of phosphorus was attributed to the movement of phosphoric acid-char layer, and the movement of phosphoric acid-char layer was caused by the release of NH_3 and H_2O generated by decomposition of APP and epoxy resin [50, 51]. According to our previous research [24], the bond energy of P–O was higher than the bond energy of Si–O. The Na_2O -rich area formed because O of Na–O was easily

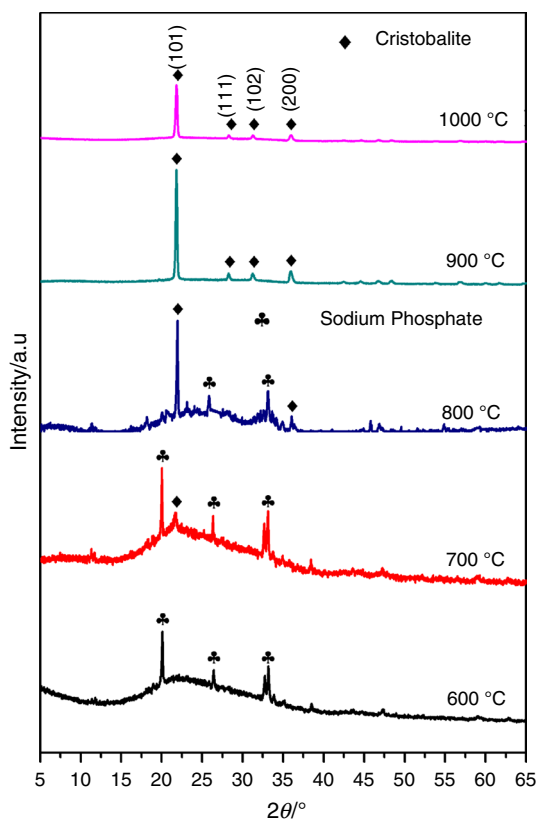


Fig. 10 XRD patterns of sample EPSA fired at different temperatures

captured by P_2O_5 , resulting in the sodium in the SGF migrated into the phosphate phase during the migration of phosphorus. Therefore, elemental migration promoted the formation of Si-rich regions in SGF. The Si–O non-bridging oxygen bond in the Si-rich region converted into Si–O bridging oxygen bond at high temperatures, which was beneficial to promote the amorphous silica convert into crystal in this region [51].

However, the P–Na region that migrated to the surface converted to phosphate phase, and phase separation provided

the possibility of crystal formation. Moreover, the epoxy composite can still maintain its original shape without melting collapse at high temperatures due to the precipitation of crystals.

In order to further investigate the elemental distribution of the residue, the internal zone and surface zone of the EPSA fired at 1000 °C was tested as shown in Fig. 12. The spectrum (Fig. 12a) showed that internal zones were mainly composed of silicon and oxygen, and the mass ratio of the two elements was close to the mass ratio of Si to O in SiO_2 . There were still a small amount of phosphorus and sodium elements presented, which could be caused by incomplete phase separation. Meanwhile, the elements of the surface zones were mainly phosphorus and sodium, and the mass ratio of phosphorus to sodium was close to the mass ratio of P and Na in $Na_4P_2O_7$. It was also inevitable that a small amount of silicon remained on the residue surface.

Phase separation and crystallization reaction mechanisms

The process of phase separation and crystallization reaction within the EPSA is proposed in Fig. 13. Firstly, the thermal decomposition of epoxy resin and APP in EPSA occurred at the beginning of firing, which produced H_2O , NH_3 , and CO_2 . Then, phosphoric acid was formed during the decomposition of APP, and the char decomposed by epoxy resin was coated by the formed phosphoric acid. Successively, the phosphoric acid-char layer structure was produced. As the temperature was further increased, phosphorus oxides were generated. The generation of NH_3 and H_2O in the composite as well as the thermal driving force promoted the migration of the phosphoric acid-char layer. The phosphoric acid-char layer began to migrate toward the surface of the residue due to the driving force of the gases and heat, and the content of phosphorus element on the surface was increased. Meanwhile, the sodium in the SGF migrated into the phosphate phase during the process

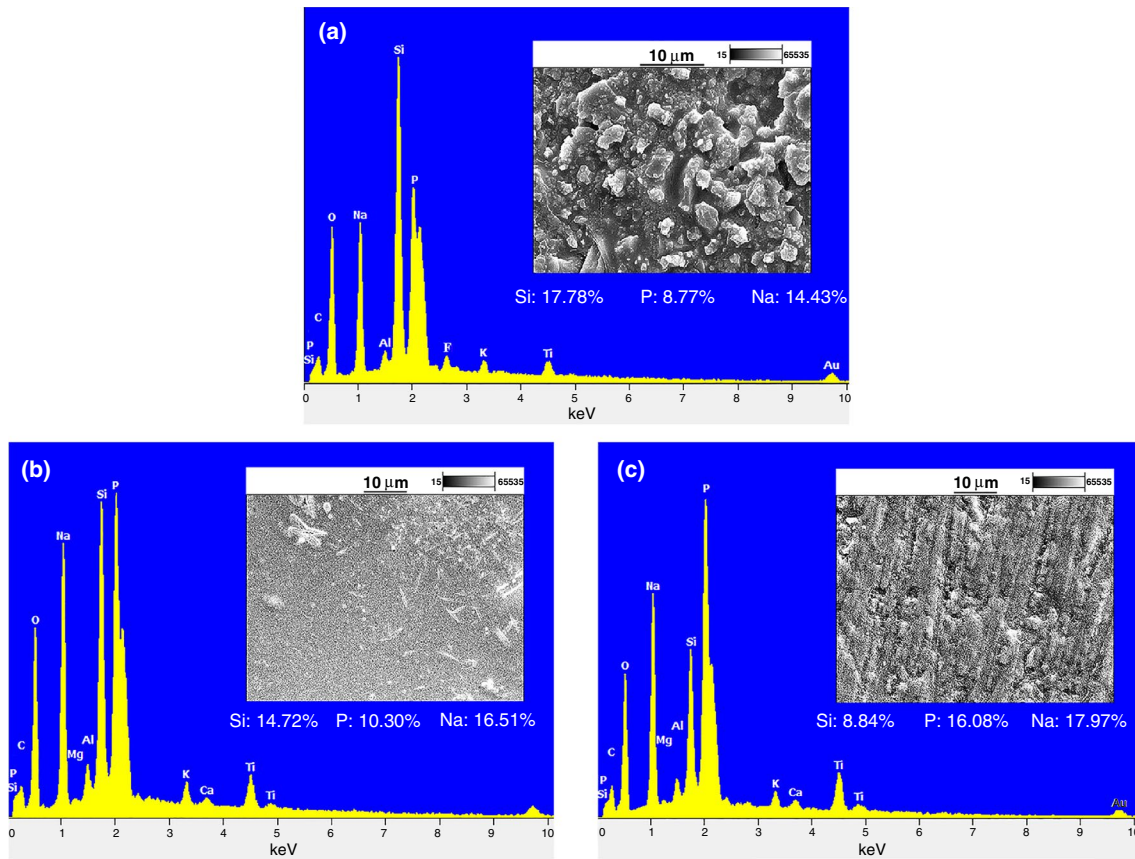


Fig. 11 EDX spectra of EPSA fired at 600 °C (a), 800 °C (b), and 1000 °C (c)

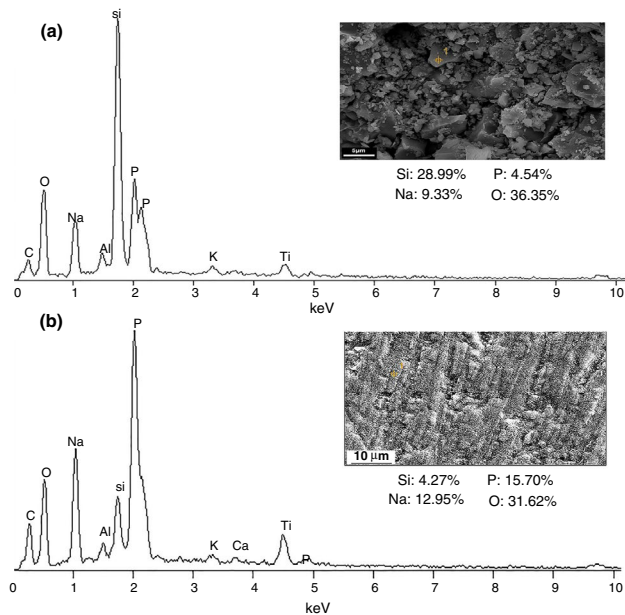


Fig. 12 The elemental content of internal (a) and surface (b) of the EPSA fired at 1000 °C

of phosphoric acid-char layer migration, because the bond energy of P–Na was higher than the bond energy of Si–Na. The P–Na region that migrated to the surface converted to a phosphate phase, forming a sodium pyrophosphate phase. Finally, a Si-rich region was formed in the SGF after the sodium migrated to the surface to form a phosphate phase. The Si–O non-bridging oxygen bond in the system was converted into Si–O bridging oxygen bond at high temperature, so the amorphous silica in this region was converted into cristobalite phase. This process showed that phase separation provided the conditions for the crystallization reaction.

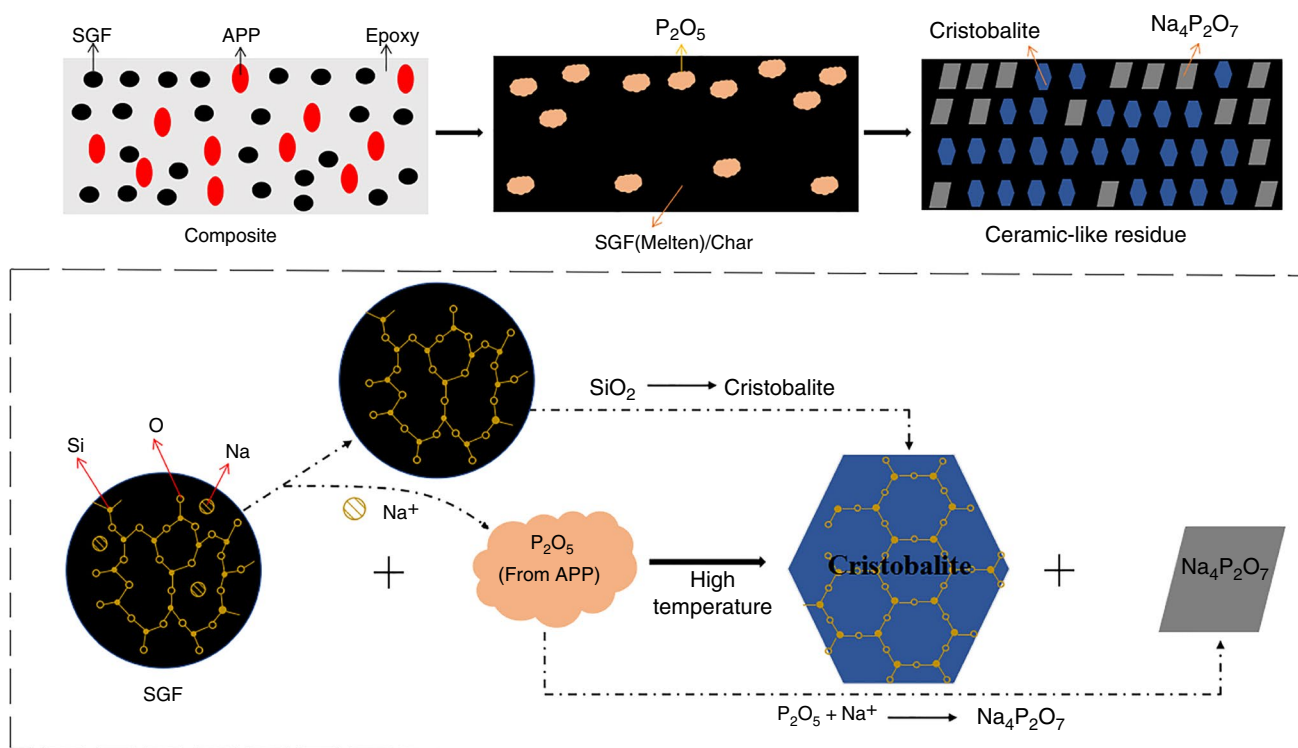


Fig. 13 Schematic illustrations of phase separation and crystallization reaction mechanisms of epoxy composite fired at high temperatures

Conclusions

In this work, a novel epoxy composite with flame retardance and high fire resistance was prepared by adding SGF and APP into the epoxy resin. The addition of SGF and APP as well as the formation of residue improved the flame retardance of the epoxy composite. The improvement of flame retardance and high fire resistance of the epoxy composite mainly benefited from the phase separation and crystallization reactions between APP and SGF during the composite firing process. The flexural strength of composite residue formed at different temperatures (600–1000 °C) kept at a relatively high level, and the original shape of the composite cannot deform seriously at high temperatures. The essential precondition for the phase separation was that the interplay between the epoxy resin matrix and APP at high temperature. The essential reason for the crystallization reactions was that sodium from SGF was captured by phosphoric acid during the phosphoric acid migration process. The migration of sodium made the transformation of amorphous silica to cristobalite crystal easier at high temperatures.

Acknowledgements This work was financially supported by National Natural Science Foundation of China (No. 51703096), China Postdoctoral Science Foundation (2018M64229), the Priority Academic Program Development of Jiangsu Higher Education Institutions (PAPD) and Industry Foresight and Generic Key Technology of Suqian (H201816).

References

- Xu MJ, Zhao W, Li B. Synthesis of a novel curing agent containing organophosphorus and its application in flame-retarded epoxy resins. *J Appl Polym Sci*. 2014;131:1–12. <https://doi.org/10.1002/app.41159>.
- Gu JW, Liang C, Zhao X, et al. Highly thermally conductive flame-retardant epoxy nanocomposites with reduced ignitability and excellent electrical conductivities. *Compos Sci Technol*. 2017;139:83–9. <https://doi.org/10.1016/j.compscitech.2016.12.015>.
- Wang N, Teng HW, Li L, Zhang J, Kang P. Synthesis of phosphated K-carrageenan and its application for flame-retardant waterborne epoxy. *Polymers*. 2018;10:1268. <https://doi.org/10.3390/polym10111268>.
- Chen ZK, Yang G, Yang JP, Fu SY, Ye L, Huang YG. Simultaneously increasing cryogenic strength, ductility and impact resistance of epoxy resins modified by n-butyl glycidyl ether. *Polymer*. 2009;50:1316–23. <https://doi.org/10.1016/j.polymer.2008.12.048>.
- Zhang JH, Kong QH, Wang DY. Simultaneously improving the fire safety and mechanical properties of epoxy resin with Fe-CNTs via large-scale preparation. *J Mater Chem A*. 2018;6:6376. <https://doi.org/10.1039/c7ta10961j>.
- Guan FL, Gui CK, Zhang HB, Jiang ZG, Jiang Y, Yu ZZ. Enhanced thermal conductivity and satisfactory flame retardancy of epoxy/alumina composites by combination with graphene nanoplatelets and magnesium hydroxide. *Compos Part B*. 2016;98:134–40. <https://doi.org/10.1016/j.compositesb.2016.04.062>.
- Müller P, Morys M, Sut A, Jäger C, Illerhaus B, Schartel B. Melamine poly(zinc phosphate) as flame retardant in epoxy resin: decomposition pathways, molecular mechanisms

- and morphology of fire residues. *Polym Degrad Stabil.* 2016;130:307–19. <https://doi.org/10.1016/j.polymdegradstab.2016.06.023>.
8. Lu SY, Hamerton I. Recent developments in the chemistry of halogen-free flame retardant polymers. *Prog Polym Sci.* 2002;27:1661–712. [https://doi.org/10.1016/s0079-6700\(02\)00018-7](https://doi.org/10.1016/s0079-6700(02)00018-7).
 9. Wang ZH, Wei P, Qian Y, Liu JP. The synthesis of a novel graphene-based inorganic–organic hybrid flame retardant and its application in epoxy resin. *Compos Part B.* 2014;60:341–9. <https://doi.org/10.1016/j.compositesb.2013.12.033>.
 10. Guo WW, Yu B, Yuan Y, Song L, Hu Y. In situ preparation of reduced graphene oxide/DOPO-based phosphonamidate hybrids towards high-performance epoxy nanocomposites. *Compos Part B.* 2017;123:154–64. <https://doi.org/10.1016/j.compositesb.2017.05.024>.
 11. Gu JW, Dang J, Wu YL, Xie C, Han Y. Flame-retardant, thermal, mechanical and dielectric properties of structural non-halogenated epoxy resin composites. *Polym Plast Technol.* 2012;51:1198–203. <https://doi.org/10.1080/03602559.2012.694951>.
 12. Mansouri J, Burford RP, Cheng YB, Hanu L. Formation of strong ceramified ash from silicone-based compositions. *J Mater Sci.* 2005;40:5741–9. <https://doi.org/10.1007/s10853-005-1427-8>.
 13. Hanu LG, Simon GP, Mansouri J, Burford RP, Cheng YB. Development of polymer–ceramic composites for improved fire resistance. *J Mater Process Tech.* 2004;153:401–7. <https://doi.org/10.1016/j.jmatprotec.2004.04.104>.
 14. Li YM, Deng C, Wang YZ. A novel high-temperature-resistant polymeric material for cables and insulated wires via the ceramization of mica-based ceramifiable EVA composites. *Compos Sci Technol.* 2016;132:116–22. <https://doi.org/10.1016/j.compscitech.2016.07.007>.
 15. Anyszka R, Bielinski DM, Pedzich Z, Szumera M. Influence of surface-modified montmorillonites on properties of silicone rubber-based ceramizable composites. *J Therm Anal Calorim.* 2015;119:111–21. <https://doi.org/10.1016/j.ceramint.2012.07.109>.
 16. Wang JH, Ji CT, Yan YT, Zhao D, Shi LY. Mechanical and ceramifiable properties of silicone rubber filled with different inorganic fillers. *Polym Degrad Stabil.* 2015;121:149–56. <https://doi.org/10.1016/j.polymdegradstab.2015.09.003>.
 17. Hu S, Chen F, Li JG, Shen Q, Huang ZX, Zhang L. The ceramifying process and mechanical properties of silicone rubber/ammonium polyphosphate/aluminium hydroxide/mica composites. *Polym Degrad Stabil.* 2016;126:196–203. <https://doi.org/10.1016/j.polymdegradstab.2016.02.010>.
 18. Guo JH, Gao W, Wang Y, Liang D, Li HJ, Zhang X. Effect of glass frit with low softening temperature on the properties, microstructure and formation mechanism of polysiloxane elastomer-based ceramizable composites. *Polym Degrad Stabil.* 2017;136:71–9. <https://doi.org/10.1016/j.polymdegradstab.2016.12.012>.
 19. Shi MX, Chen X, Fan SS, Shen S, Liu TX, Huang ZX. Fluxing agents on ceramification of composites of MgO–Al₂O₃–SiO₂/Boron phenolic resin. *J of Wuhan University of Technology Mater Sci.* 2018;33:381–8. <https://doi.org/10.1007/s11595-018-1833-8>.
 20. Mansouri J, Wood CA, Roberts K, Cheng YB, Burford RP. Investigation of the ceramifying process of modified silicone–silicate compositions. *J Mater Sci.* 2007;42:6046–55. <https://doi.org/10.1007/s10853-006-1163-8>.
 21. Di HW, Deng C, Li RM, Dong LP, Wang YZ. A novel EVA composite with simultaneous flame retardation and ceramifiable capacity. *Rsc Adv.* 2015;5:51248–57. <https://doi.org/10.1039/C5RA05781G>.
 22. Imiela M, Anyszka R, Bieliński DM, Pędzich Z, Zarzecka NM, Szumera M. Effect of carbon fibers on thermal properties and mechanical strength of ceramizable composites based on silicone rubber. *J Therm Anal Calorim.* 2016;124:197–203. <https://doi.org/10.1007/s10973-015-5115-x>.
 23. Lou FP, Wu K, Wang Q, Qian ZY, Li SJ, Guo WH. Improved flame-retardant and ceramifiable properties of EVA composites by combination of ammonium polyphosphate and aluminum hydroxide. *Polymers.* 2019;11:125. <https://doi.org/10.3390/polym11010125>.
 24. Zhao D, Shen YC, Wang T. Ceramifiable EVA/APP/SGF composites for improved ceramifiable properties. *Polym Degrad Stabil.* 2018;150:140–7. <https://doi.org/10.1016/j.polymdegradstab.2018.02.006>.
 25. Gong XH, Shen YC, Wang TW. Improved ceramifiable properties of EVA composites with whitened and capsulized red phosphorus (WCRP). *RSC Adv.* 2016;6:96984–9. <https://doi.org/10.1039/C6RA22126B>.
 26. Gong XH, Wu TY, Ma J, Zhao D, Shen YC, Wang TW. Improved self-supporting property of ceramifying silicone rubber composites by forming crystalline phase at high temperatures. *J Alloy Compd.* 2017;706:322–9. <https://doi.org/10.1016/j.jallcom.2017.02.252>.
 27. Gong XH, Wang TW. Optimisation of the ceramic-like body for ceramifiable EVA-based composites. *Sci Eng Compos Mater.* 2017;24:599–607. <https://doi.org/10.1515/secm-2015-0093>.
 28. Lou FP, Yan W, Guo WH, Wei T, Li QY. Preparation and properties of ceramifiable flame-retarded silicone rubber composites. *J Therm Anal Calorim.* 2017;130:813–21. <https://doi.org/10.1007/s10973-017-6448-4>.
 29. Dong LP, Deng C, Li RM, Cao ZJ, Lin L, Che L, Wang YZ. Poly(piperazinyl phosphamide): a novel highly-efficient charring agent for an EVA/APP intumescent flame retardant system. *Rsc Adv.* 2016;6:30436–44. <https://doi.org/10.1039/C6RA00164E>.
 30. Liao SF, Deng C, Huang SC, Cao JY, Wang YZ. An efficient halogen-free flame retardant for polyethylene: piperazine modified ammonium polyphosphates with different structures. *Chinese J Polym Sci.* 2016;34:1339–53. <https://doi.org/10.1007/s10118-016-1855-8>.
 31. Kong QH, Sun YL, Zhang CJ, Guan HM, Zhang JH, Wang DY, Zhang F. Ultrathin iron phenyl phosphonate nanosheets with appropriate thermal stability for improving fire safety in epoxy. *Compos Sci Technol.* 2019;182:107748. <https://doi.org/10.1016/j.compscitech.2019.107748>.
 32. Yu ZL, et al. Fire-retardant and thermally insulating phenolic-silica aerogels. *Angewandte Chemie Int Edition.* 2018;57:4538–42. <https://doi.org/10.1002/anie.201711717>.
 33. Yang XT, Tang L, Guo YQ, Liang CB, Zhang Q, Kou KC, Gu JW. Improvement of thermal conductivities for PPS dielectric nanocomposites via incorporating NH₂-Poss functionalized nBN fillers. *Compos Part A.* 2017;101:237–42. <https://doi.org/10.1016/j.compositesa.2017.06.005>.
 34. Zhang YW, Shen YC, Shi KX, Wang TW, Harkin JE. Constructing a filler network for thermal conductivity enhancement in epoxy composites via reaction-induced phase separation. *Compos Part A.* 2018;110:62–9. <https://doi.org/10.1016/j.compositesa.2018.04.009>.
 35. Xiong YL, Shen Q, Chen F, Luo GQ, Yu K, Zhang LM. High strength retention and dimensional stability of silicone/alumina composite panel under fire. *Fire Mater.* 2012;36:254–63. <https://doi.org/10.1002/fam.1107>.
 36. Anyszka R, Bielinski DM, Pedzich Z, Rybinski P, Imiela M, Sicinski M, Zarzecka-Napierała M, Gozdek T, Rutkowski P. Thermal stability and flammability of styrene-butadiene rubber-based (SBR) ceramifiable composites. *Materials.* 2016;9:604–16. <https://doi.org/10.3390/polym9110615>.
 37. Xu J, Wang YJ, Tan Y, Qi M, Chen L, Wang YZ. A novel and feasible approach for one-pack flame-retardant epoxy resin with

- long pot life and fast curing. *Chem Eng J.* 2018;337:30–9. <https://doi.org/10.1016/j.cej.2017.12.086>.
38. Jiang WZ, Hao JW, Han ZD. Study on the thermal degradation of mixtures of ammonium polyphosphate and a novel caged bicyclic phosphate and their flame retardant effect in polypropylene. *Polym Degrad Stabil.* 2012;97:632–7. <https://doi.org/10.1016/j.polymdegradstab.2012.01.001>.
 39. Cinausero N, Azema N, Lopez-Cuesta JM, Cochez M, Ferriol M. Synergistic effect between hydrophobic oxide nanoparticles and ammonium polyphosphate on fire properties of polymethyl methacrylate and polystyrene. *Polym Degrad Stabil.* 2011;96:1445–54. <https://doi.org/10.1016/j.polymdegradstab.2011.05.008>.
 40. Kanai H, Sullivan V, Auerbach A. Impact modification of engineering thermoplastics. *J Appl Polym Sci.* 1994;53:527–41. <https://doi.org/10.1002/app.1994.070530507>.
 41. Hsiue GH, Wei HF, Shiao SJ, Kuo WJ, Sha YA. Chemical modification of dicyclopentadiene-based epoxy resins to improve compatibility and thermal properties. *Polym Degrad Stabil.* 2001;73:309–18. [https://doi.org/10.1016/S0141-3910\(01\)00092-1](https://doi.org/10.1016/S0141-3910(01)00092-1).
 42. Ye CS, Chen LX, Bai XG, Bao XT. Research progress of flame retardant silicon-containing epoxy resin system. *Shanxi Chemical Industry.* 2009;29:33–7.
 43. Wu CL, Wang BB, Tao R, Fang LW, Li HX. Study of mineral structure transformation of coal Ash with high ash melting temperature by XPS. *Spectrosc Spectr Anal.* 2018;38:2296–301. [https://doi.org/10.3964/j.issn.1000-0593\(2018\)07-2296-06](https://doi.org/10.3964/j.issn.1000-0593(2018)07-2296-06).
 44. Dong S, Pang X. Xps analysis of phosphorylation layer on iron surface. *Mater Protec.* 1984;10:16577.
 45. Ma HB, Li J, Ren TH. Tribological behavior s and film analysis of two ashless phosphorus/sulfur-containing additives in rapeseed oil. *Acta Phys Chim Sin.* 2008;24:799–804.
 46. Mansouri J, Burford RP, Cheng YB. Pyrolysis behaviour of silicone-based cer-amifying composites. *Mater Sci Eng A Struct Mater Proper Microstruct Process.* 2006;425(1–2):7–14. <https://doi.org/10.1016/j.msea.2006.03.047>.
 47. Honma T, Sato A, Ito N, Togashi T, Shinozaki K, Komatsu T. Crystallization behavior of sodium iron phosphate glass for sodium ion batteries. *J Non-Cryst Solids.* 2014;404:26–31. <https://doi.org/10.1016/j.jnoncrysol.2014.07.028>.
 48. Dong WX, Bao QF, Gu X, Shen H, Yang J. Dry-pressing preparation of mullite columnar structure using waste gangue during firing and its properties. *J Ceram Soc Jpn.* 2017;125:75–8. <https://doi.org/10.2109/jcersj2.16258>.
 49. Ou YX. Flame retardant. 4th ed. Beijing: National Defense Industry Press; 2009.
 50. Levchik SV, Camino G, Levchik GF, Costa L. Mechanism of action of phosphorus-based flame retardants in nylon 6. I. ammonium polyphosphate. *Fire Mater.* 1995;19:1–10.
 51. Zhang QT. Inorganic materials science foundation. 1st ed. Shanghai: East China University Sci Tech Press; 2007.

Publisher's Note Springer Nature remains neutral with regard to jurisdictional claims in published maps and institutional affiliations.

Affiliations

Dong Zhao^{1,2} · Wei Liu^{1,2} · Yucai Shen^{1,2} · Tingwei Wang^{1,3}

✉ Yucai Shen
ycshen@njtech.edu.cn

✉ Tingwei Wang
wangtw@njtech.edu.cn

¹ College of Material Science and Engineering, Nanjing Tech University, Nanjing 211816, China

² Jiangsu Collaborative Innovation Center for Advanced Inorganic Function Composites, Nanjing 211816, China

³ Suqian Advanced Materials Institute of Nanjing Tech University, Suqian 223800, China